*Minireview*

# Imaging and detection of long-lived fluorescence probes in presence of highly emissive and scattering background

**Luca Ceresa, Jose Chavez, Emma Kitchner, Joseph Kimball, Ignacy Gryczynski and Zygmunt Gryczynski**

Department of Physics and Astronomy, Texas Christian University, Fort Worth, TX 76109, USA
Corresponding author: Luca Ceresa. Email: Luca.ceresa@tcu.edu

### Impact Statement

Fluorescence imaging is a diagnostic modality that offers high sensitivity and minimally invasive detection. Practical medical detection/imaging is done on a highly scattering and emissive biological medium-like tissue, physiological fluids, or cellular environment. The fundamental limiting factor for any biomedical imaging and detection is the signal-to-background ratio (SBR). Our work presents a simple and effective solution to increase the SBR and improve image quality in highly scattering media. The innovation of our approach is the use of excitation pulse sequences with long-lived fluorescence emitters that lowers the relative background contribution and allows for simple image subtraction to decrease background and scattering contributions. Practical applications can easily be realized with currently available laser drivers and time-resolved detectors or cameras. Our approach shifts the attention from improving the brightness of fluorescence probes to developing a technological approach that suppresses background contribution when long-lived fluorescence probes are used combined with time-gated detection.

### Abstract

Optical biomedical imaging and diagnostics is a rapidly growing field that provides both structural and functional information with uses ranging from fundamental to practical clinical applications. Nevertheless, imaging/visualizing fluorescence objects with high spatial resolution in a highly scattering and emissive biological medium continues to be a significant challenge. A fundamental limiting factor for imaging technologies is the signal-to-background ratio (SBR). For a long time to improve the SBR, we tried to improve the brightness of fluorescence probes. Many novel fluorophores with improved brightness (almost reaching the theoretical limit), redshifted emission, highly improved photostability, and biocompatibility greatly helped advance fluorescence detection and imaging. However, autofluorescence, scattering of excitation light, and Raman scattering remain fundamental limiting problems that drastically limit detection sensitivity. Similarly, significant efforts were focused on reducing the background. High-quality sample purification eliminates the majority of autofluorescence background and in a limited confocal volume allows detection to reach the ultimate sensitivity to a single molecule. However, detection and imaging in physiological conditions does not allow for any sample (cells or tissue) purification, forcing us to face a fundamental limitation. A significant improvement in limiting background can be achieved when fluorophores with a long fluorescence lifetime are used, and time-gated detection is applied. However, all long-lived fluorophores present low brightness, limiting the potential improvement. We recently proposed to utilize multipulse excitation (burst of pulses) to enhance the relative signal of long-lived fluorophores and significantly improve the SBR. Herein, we present results obtained with multipulse excitation and compare them with standard single-pulse excitation. Subtraction of images obtained with a single pulse from those obtained with pulse burst (differential image) highly limits background and instrumental noise resulting in more specific/sensitive detection and allows to achieve greater imaging depth in highly scattering media, including skin and tissue.

**Keywords:** Multipulsing, DNA intercalator, bioimaging, biomedical, time-resolved imaging, fluorescence spectroscopy

***Experimental Biology and Medicine* 2022; 247: 1840–1851. DOI: 10.1177/15353702221112121**

## Introduction

Fluorescence is a process occurring after absorption of a photon when the excited chromophore releases part of the absorbed energy after some duration of time in the form of a typically lower energy photon (i.e. longer wavelength).[1–4] The average time duration between the absorption and emission process for a fluorophore is called the fluorescence lifetime. It is important to remember that the process of photon emission after excitation is a statistical phenomenon, and fluorescence lifetime represents the time after which 63.2% of the excited chromophores have returned to the ground state (both in radiative [$\Gamma$] and non-radiative [$k_{nr}$] pathways). As a result, a fluorescence probe will be characterized by a specific fluorescence lifetime, $\tau$, and a specific quantum yield (QY) as defined by[1–4]

$$\tau = \frac{1}{\Gamma + k_{nr}} \quad \text{and} \quad \text{QY} = \frac{\Gamma}{\Gamma + k_{nr}} \tag{1}$$

ISSN 1535-3702

where Γ is the radiative decay rate and $k_{nr}$ represents all non-radiative decay rates. For the majority of typical fluorophores, the fluorescence lifetime will range from sub-nanoseconds to a few nanoseconds, and only a handful of emitters will have a longer fluorescence lifetime. Long-lifetime emitters may have lifetimes in the range of 20 ns like ADOTA[5,6] or ethidium bromide when intercalated to DNA,[7,8] to hundreds of nanoseconds and microseconds like ruthenium metal–ligand complexes[9–12] (MLCs) and some metal clusters,[13,14] or even milliseconds with lanthanide-based emitters.[15–18] Some quantum dot-type emitters will also have long emissive lifetimes over 20 ns.[19,20] A separate case is represented by the phosphorescence process, which can have very long emission lifetimes.[20–23] Regardless of the nature of the fluorophore, a common characteristic of long lifetime emitters is typically a very low brightness, drastically limiting the uses of such probes. This low brightness is dictated by quantum mechanical principles.[24] The long fluorescence lifetime is typically a consequence of a very low extinction coefficient, or very low QY, or both.

Because of its sensitivity and flexibility, fluorescence spectroscopy has been widely used in biomedical diagnostics, real-time visualization of biomedical processes, and imaging.[1–4] It offers excellent sensitivity and high resolution. However, the sensitivity of any imaging method is limited by the background signal, and the highest sensitivity at the level of a single molecule can only be effective in a background-free environment.[16,17,25] Unfortunately, the background is a primary concern for practical diagnostics applications in physiological conditions.[25–27] To reduce the background contribution for fluorescence detection, much effort has been focused on developing near-infrared (NIR) fluorophores and fluorescent nanomaterials.[28–30] The advantage of moving the detection toward the red/NIR range is that the autofluorescence from biological components and tissue significantly decreases, and a higher penetration depth can be achieved. Even though this allows for a great increase of sensitivity, scattering of excitation light and especially Raman scattering (mostly of water) remains a significant problem. Unfortunately, even if most red/NIR emitters present a good QY, their Stokes shift between absorption and emission spectra is very small, and fluorescence lifetimes are very short. As a result, distinguishing the true emission signal from excitation light scattering and Raman background is a significant detection barrier. These are the reasons why chemiluminescent (CL) materials usually offer better sensitivity (luminescence signal does not require excitation light and is generated on optically background-free conditions), and a higher penetration depth can be reached.[31–34] Two-photon excitation of fluorescence allows to reach deeper into cellular systems, but autofluorescence background, scattering background, and background from second harmonics remain a problem.

Despite the brightness limitation, long-lived probes attract more and more attention and hold great promise for practical imaging and diagnostic applications. A considerable advantage of long-lived probes is their possibility to temporarily separate their emission from fast processes like scattering, Raman scattering, or typical nanosecond fluorescence.[16,17] For this reason, a simple time-gating approach has been used to suppress short-lived signals (scattering and background emission). Time gating is a passive approach that always leads to not only a loss of the short-lived signal but also, however smaller, a loss of the probe signal. Such an approach has proven successful for very long fluorescence lifetimes, as observed with lanthanide-based probes.[16,17]

Most tissues and biological/physiological fluids are highly scattering and weakly emissive systems for which the emissive lifetimes are short (below 2 ns) with only a minor contribution of longer (4–7 ns) lifetime components.[27,35–37] In addition, the probability of scattering interaction with tissue components exceeds that of medium absorption by at least an order of magnitude, leading to a much weaker excitation and diffusion of emission light.

As schematically shown in Figure 1, fluorescence-based detection in a complex medium presents multiple types of processes that may perturb detection and should be considered. First, the excitation light is reflected and scattered, which attenuates and diffuses the excitation of the chromophore. In addition, the emission of photons of different wavelengths is accompanied by their scattering and diffusion.

Since the autofluorescence background presents a short picosecond to nanoseconds fluorescence lifetime and scattering is an instantaneous process, the use of long-lived emitters and time-gated detection allows for significant improvement in detection and imaging sensitivity. To mitigate the low brightness of long-lived chromophores, we recently proposed an approach based on multipulse pumping that greatly increases the observed signal from the long-lived probe compared to the short-lived background. This increase can be an order of magnitude when long lifetime dyes are used. When using multipulse pumping and time-gated detection (MPPTGD), even for relatively short probe lifetimes in the range of 20 ns, we increased the detection sensitivity by two orders of magnitude.[7,38]

We now realize that we can utilize this technology for practical biomedical imaging. We can produce almost background-free images using pulsing technology and simple image manipulation. In effect, we can precisely extract the signal associated with the long-lived component and eliminate the undesired short-lived components, scattering, and background, which vastly increases detection sensitivity and precision of imaging. In scattering systems like tissue, we reject the scattered and diffusing photons and significantly increase the detection depth. In practice, we can easily extract the signal through the skin even with ultraviolet (UV)/blue excitation and visible observation. Using red emitters, we expect to be able to optically reach up to a centimeter depth.

## Main text

### Theoretical considerations

Some fluorescence probes like metal-ligand emitters and many quantum dots offer long fluorescence lifetimes (over 100 ns), but they present a relatively low brightness (small extinction coefficient and low QY).[2,24] Low brightness is a significant disadvantage, but a long fluorescence lifetime offers great potential when time-gated detection is applied. During the time delay between the excitation pulse and gate time opening (beginning of the detection), both signal

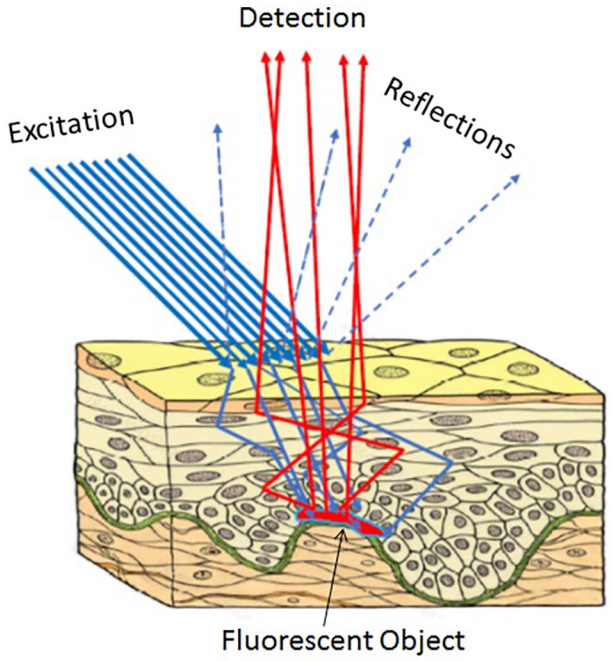


**Figure 1.** Schematic of excitation and emission of a fluorescent object in tissue. Excitation beam (blue), ballistic excitation photons reaching the sample, scattered photons reaching the sample, specular reflectance, and emission (red) – direct and diffused (scattered). (A color version of this figure is available in the online journal.)

components (from the probe and the background) exponentially decay. Since the short-lived background components from tissue and cells decay faster (with lifetimes below 10 ns),[27,38] the long delay after the excitation pulse improves the ratio between the useful probe signal and the unwanted background. However, the observable probe signal consistently decreases with time delay, limiting the amount of signal detected from the probe. This limits the detection sensitivity, especially when the brightness of the probe is very low. To increase the available signal from the long-lived probe, we developed a multipulse pumping approach that greatly increases the initial signal (relative contribution) of the long lifetime component without changing the contribution from the short-lived components. In this case, the combination of multipulse pumping with time-gated detection can result in a few orders of magnitude detection sensitivity enhancement.[7]

Let us consider the intensity decay of a system that consists of two components, a background that has a short fluorescence lifetime $\tau_s$ (e.g. <5 ns) and is characterized by a broad single emission band (Gaussian) with a single maximum at 550 nm, and a probe emission characterized by a long fluorescence lifetime $\tau_l$ (e.g. 300 ns). The simulated normalized emission spectra of the background and probe are shown in Figure 2(A). For clarity of presentation, the probe emission has two peaks at 540 and 630 nm to be easily distinguished from the background emission, as presented in Figure 2(A).

For our considerations, we assume that the background emission is about 10 times stronger than the probe signal and overlays the entire probe emission. The expected steady-state emission of background, probe, and their composition

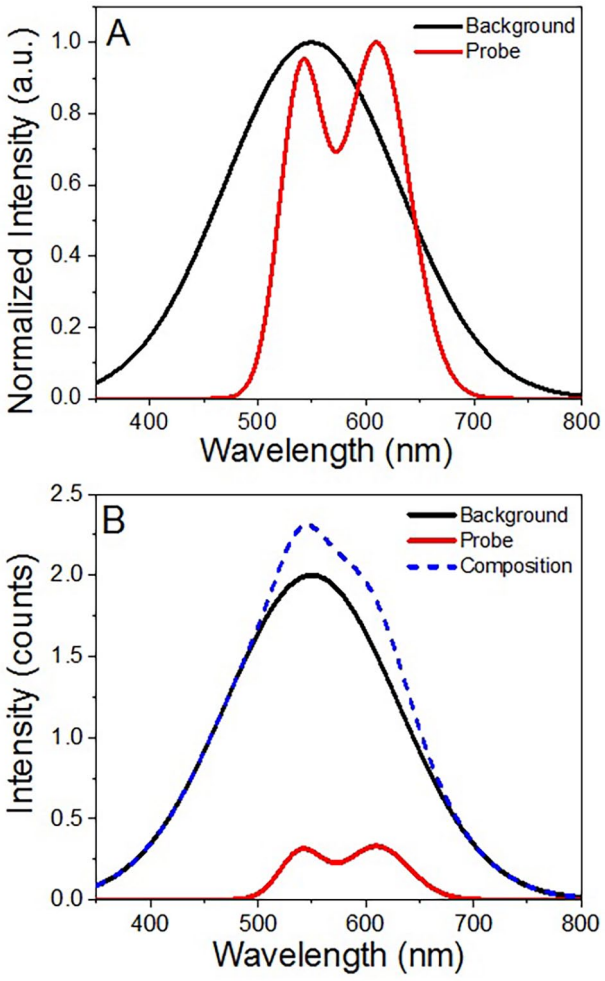


**Figure 2.** Simulated normalized emission spectra of background and probe (A) and expected steady-state emission of background, probe, and their composition (B). (A color version of this figure is available in the online journal.)

are presented in Figure 2(B). The expected cumulative emission from the probe and background is presented as a dashed line in Figure 2(B). Since we assumed that the background contribution to the steady-state intensity is 10 times greater, the cumulative emission is entirely dominated by the background. For known emission spectra, the cumulative emission can be precisely decomposed to separate background and probe components. However, if a spectrum is unknown (a frequent case with background emission of cells and tissue), the deconvolution will not produce satisfactory results. Also, from the point of view of imaging, a large background contribution that is larger or even comparable to the probe signal would disqualify any image analysis.

Figure 3 shows normalized (to 1 at the maximum intensity) intensity decays for the probe and background (presented in solid blue and black colors, respectively). The cumulative intensity decay is presented as a dashed red line.

To fully follow the intensity decay for a lifetime of 300 ns, we used a pulse separation of 2000 ns (500 kHz excitation laser repetition rate). Let us consider two measurements in time-correlated single photon counting (TCSPC) mode. First, emission intensity decay in a standard single-pulse excitation where the measurement is triggered by the excitation

pulse (Figure 4 [top]). The short component decays quickly, and after 20 ns, it is almost zero. Second (Figure 4 [bottom]), we present the intensity decay trace when the excitation is achieved with a burst of $N$ identical pulses ($N=4$ in the presented case) with a pulse-to-pulse separation of 25 ns (pulse-to-pulse separation for 40 MHz laser repetition rate). The repetition for the bursts is the same as for a single pulse (i.e. 500 kHz). Such a sequence of pulses is easy to realize with a modern laser driver (e.g. Sepia from PicoQuant GmbH, Berlin, Germany).

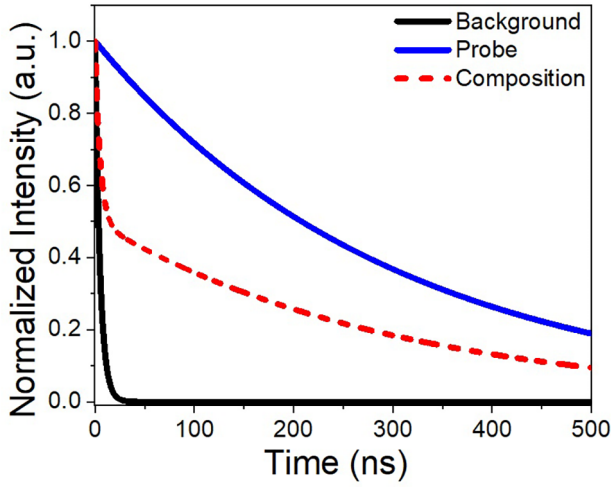


**Figure 3.** Normalized intensity decays for probe (solid blue line), background (solid black line), and cumulative intensity decay (dashed red line). (A color version of this figure is available in the online journal.)

When using TCSPC, the integrated curve under the intensity decay represents the measured steady-state intensity. When integrating over the entire time range (including pulses), the overall intensity for four pulses (the so-called steady-state intensity) is four times greater than the intensity measured with a single pulse. Also, the relative intensity contribution from long and short lifetimes for the decay of the mix is constant and independent of the number of pulses in the burst. However, TCSPC mode allows us to initiate photon counting with any wanted delay and keep the gate open for any time of our choice. Let us now assume that we initiate photon counting at time zero (as shown in Figure 4). For a single pulse, this is the arrival time of the pulse, and for the burst of pulses is the arrival time of the last pulse in the burst (the arrival time for any previous pulse $n$ in the pulse train of $N$ pulses is $(n-N)\Delta t$, where $\Delta t$ is the pulse separation). Therefore, for the four-pulse burst shown in Figure 4,

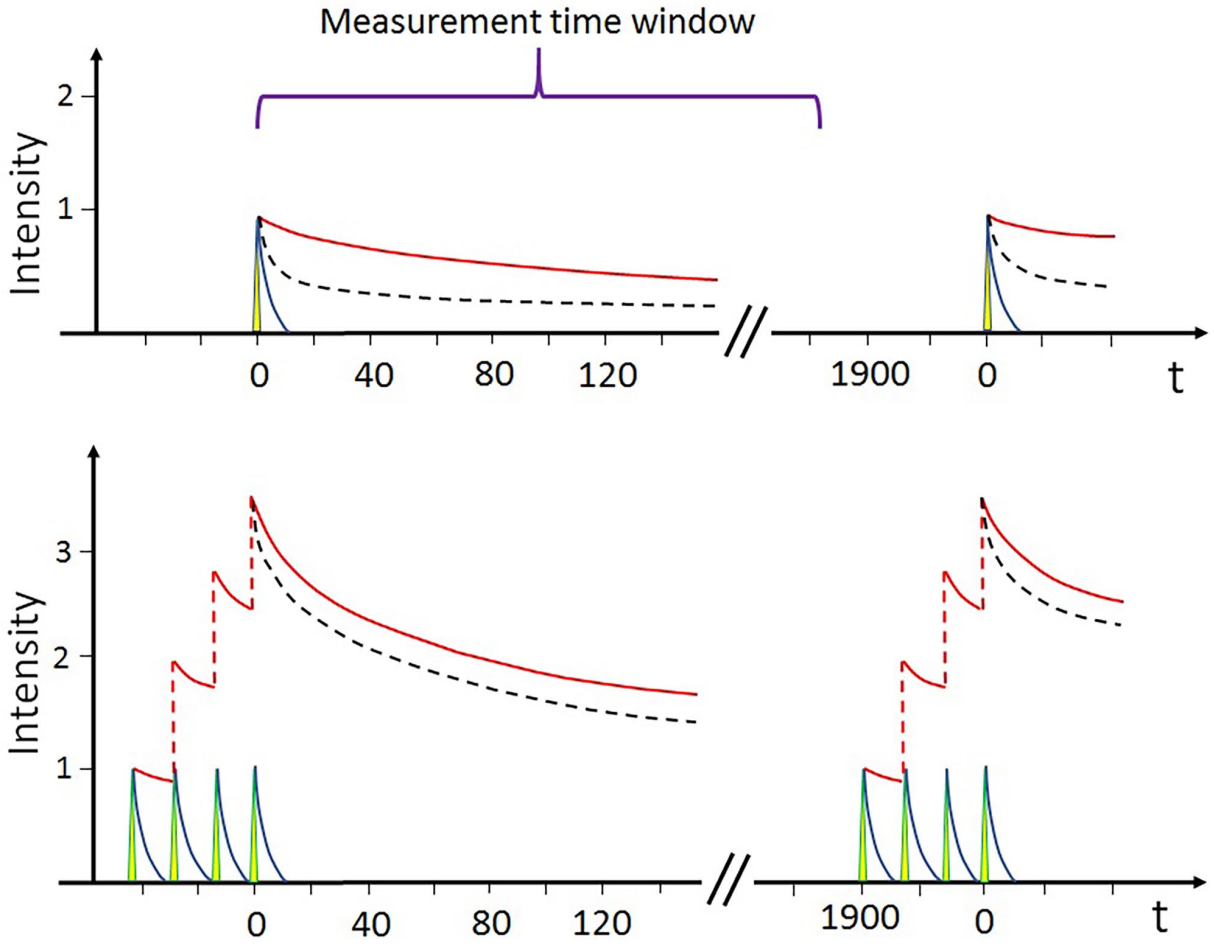


**Figure 4.** Emission intensity decay in a standard single-pulse excitation where the measurement is triggered by the excitation pulse (top). The repetition rate of 500 kHz results in a temporal spacing between pulses of 2000 ns (1900 ns is indicated as a reference). Intensity decay trace when the excitation is achieved with a burst of four identical pulses with a pulse-to-pulse separation of 25 ns (pulse-to-pulse separation for 40 MHz laser repetition rate). The additional three pulses in the burst are generated before the first one. As a result, the single pulse is always aligned with the last pulse in the burst. (A color version of this figure is available in the online journal.)

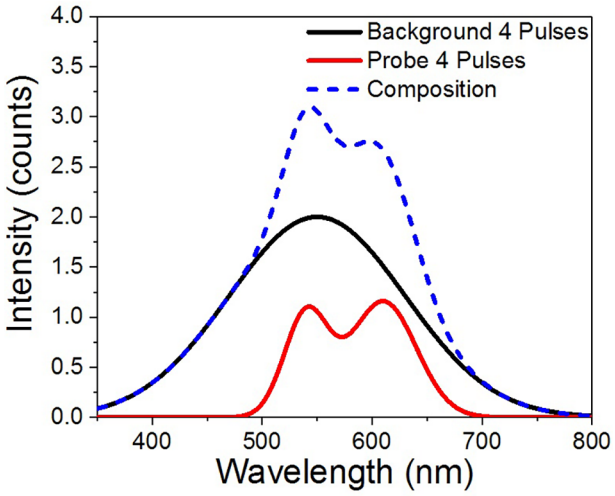


**Figure 5.** Expected signal from background (black solid line), probe (red solid line), and their composition (dashed blue line) with four pulses. The collection is initiated with the last pulse in the burst and the signal is collected for a time shorter than 1900 ns but sufficient for both background and probe to decay. (A color version of this figure is available in the online journal.)

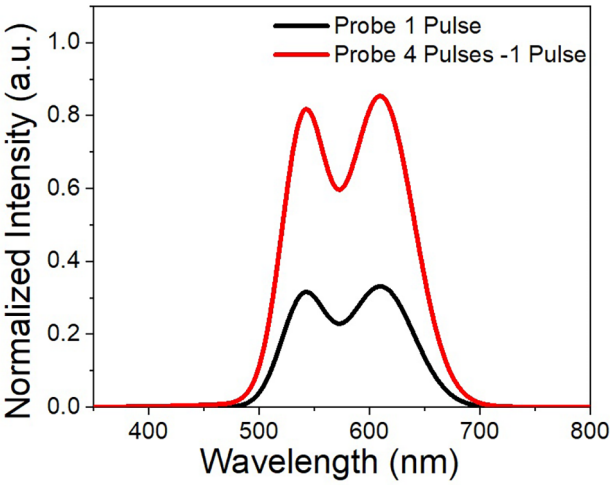


**Figure 6.** Differential spectrum obtained by subtracting the overall/total spectrum detected with a single pulse from the total spectrum obtained with a burst of four pulses (red solid line) and expected emission signal from the single-pulse excitation (black solid line). (A color version of this figure is available in the online journal.)

the first pulse arrives at a time of −75 ns. Since we do not want to collect signals during the time when the four pulses excite the sample, we keep the time of gate opening shorter than $1/\mathrm{RR} - N\Delta t$, where RR stands for the repetition rate. In this case, we will lose the intensity generated between pulses during the burst ($N\Delta t$ – in our case, four pulses – 100 ns). In practice, if the pulse separation in the burst is a few times longer than the fluorescence lifetime of the short component, the intensity of this component completely decays between each subsequent pulse. So, after the last pulse that triggers the counting, the initial intensity of the short component is comparable to the intensity with a single pulse (the initial intensity after each pulse is the same) as shown in Figure 4.

On the contrary, for the long lifetime component (much longer than the time $\Delta t$ between pulses in the burst), the population of excited probes will only decay partially, and each subsequent pulse will increase the population of excited long-lived probes. For the last pulse in the burst (time equals zero), the initial intensity of the long component is much higher. In practice, for a fluorophore that has fluorescence lifetime $\tau$, the number of excited molecules after $n$ consecutive excitation pulses in the burst can be described by[38,39]

$$N(\tau, n, \mathrm{RR}) = N_e \frac{1 - e^{-\frac{n}{\tau}\cdot\mathrm{RR}}}{1 - e^{-\frac{1}{\tau}\cdot\mathrm{RR}}} \qquad (2)$$

where RR is the repetition rate in the pulse burst, and $n$ is the number of pulses. For short fluorescence lifetimes as compared to the reciprocal of pulse repetition rate ($\tau << 1/\mathrm{RR}$), the population of excited molecules after each pulse decays to zero, and for long fluorescence lifetimes ($\tau >> 1/\mathrm{RR}$), the population of excited molecules quickly increases after each subsequent pulse.

Effectively, in the measurement window, we significantly increase the long component's detected intensity while keeping the short component at a constant level. In the discussed case of four pulses, the relative intensity of the long component increases over 3.5-fold, while the background components and any other background contributors (e.g. scattering) remain constant.

Let us now return to the experiment as presented in Figure 2(B), where the background component (short-lived component) dominates the signal. Such an overwhelming background is completely unacceptable for any practical experimental situation. The real signal is entirely buried within the background (it is about 10% of the overall measured intensity), and typical intensity imaging will not be able to reveal any appreciable changes in the probe signal. In Figure 5, we present the signal expected with four pulses where the collection is initiated with the last pulse in the burst, and the signal is collected for the same time as in Figure 2(B) (time shorter than 1900 ns but sufficient for both background and probe to decay). In this case, the detected intensity of the probe is over 3.5 times greater compared to the background. The signal from the probe is much better detectable, but it still constitutes only about 30% of the overall signal. If the signal with the single pulse and the burst of four pulses are collected in identical conditions, the increase in the overall signal with the burst is solely due to the intensity increase of the long-lived probe. All the other components (i.e. short-lived background, excitation light scattering, Raman scattering, detector noise) remain constant and are the same. We can perform a simple subtraction of the signal detected with a single pulse from the signal detected with four pulses. In this case, all constant components are nulling, and the remaining difference exclusively represents the long-lived component. In Figure 6, we present the differential spectrum obtained by subtracting the overall/total spectrum detected with a single pulse (dashed line in Figure 2(B)) from the total spectrum obtained with a burst of four pulses (Figure 5). In Figure 6, we also included the expected emission signal from the single-pulse excitation from Figure 2(B). The detected differential signal is greater than the expected signal from a single pulse, but the recovered emission spectrum is almost identical.

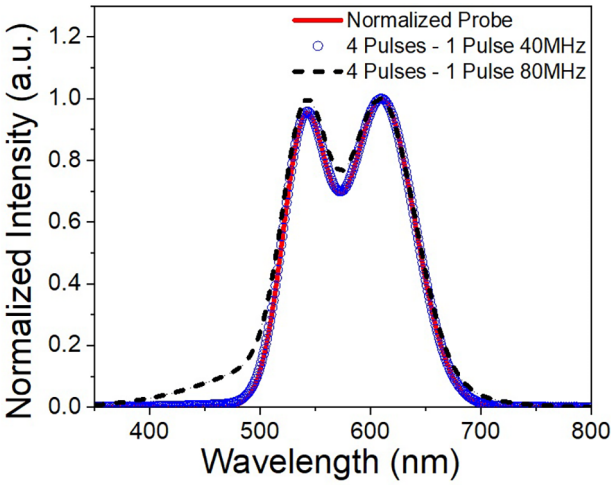


**Figure 7.** Normalized differential spectrum obtained with repetition rate of 40 MHz (blue dots), normalized differential spectrum obtained with repetition rate of 80 MHz (black dashed line), and normalized emission spectrum of the probe (red solid line). (A color version of this figure is available in the online journal.)

In Figure 7, we show the normalized differential spectrum (blue dots) and the normalized emission spectrum of the probe (solid red line). The agreement between probe emission and the differential spectrum obtained by subtraction is very good, and only a small variation can be observed at the wavelength range of background emission. We want to notice that the difference depends on the relative relation between the pulse separation in the burst and the fluorescence lifetimes of the probe and background. For example, increasing the repetition rate to 80 MHz, which results in a pulse separation of 12.5 ns, not much longer than the assumed fluorescence lifetime of the background (5 ns), results in a small deformation of the recovered spectrum. The normalized differential spectrum is shown in Figure 7 as a dashed line. The deviation from the expected probe emission spectrum is much more pronounced with the greater RR. However, even in this case, the obtained differential spectrum is very close to the expected probe emission. We want to stress that the initial contribution of the sample was only 10%.

There are a few important points to notice. First, the overall detected signal from the probe excited with the pulse burst is significantly greater than the signal detected with single-pulse excitation. Second, the differential spectrum well reflects the emission spectrum of the long-lived component (probe). Third, any noise and ambient signals are canceled by the spectra subtraction. This creates a great opportunity for image manipulation during typical tissue or cellular imaging. It is very easy to collect images with a single pulse and subsequently images with a burst of two or more pulses. There are various methods for obtaining such pulse bursts as described by us.[38–41]

However, much more effective for imaging would be to utilize the already existing technology of interleaved excitation, frequently used to perform the Förster resonance energy transfer (FRET)–based imaging.[41–43] Using modern drivers, it is easy to generate a train of pulses, and the sample is excited alternatively with a single pulse and a burst of a few pulses. In such a case, two images are collected simultaneously, and the differential image can be obtained instantaneously.[42]

## Experimental section

To test our theoretical predictions, we selected a simple system based on Rhodamine 6G (Rh) that has a short fluorescence lifetime below 5 ns and an MLC – $[Ru(bpy)_2$ (amino phenanthroline)$]^{2+}$ (Ru stands for Ruthenium) that has a much longer fluorescence lifetime (over 300 ns) but also a much lower brightness.[45] Also, due to the very long fluorescence lifetime, most of the emission is from the fully relaxed excited state. We would not expect any significant spectral modification during the emission time. First, we will demonstrate that using an approach based on a single pulse and pulse burst, we can clearly recover the Ru emission spectrum by simple subtraction of the measured single-pulse spectrum from a multipulse spectrum. The demonstration of good spectra recovery would establish a compelling case for further image analysis. We want to stress that we expect some spectral differences as observed with a single pulse or burst of pulses. The emission process is a statistical phenomenon, and even with a rather short lifetime of 5 ns, we may expect some molecules to be in the excited state after 25 ns or more. These molecules will contribute (add) to the overall spectrum observed after each pulse. The emission of such late molecules will be from a highly relaxed state that is expected to be shifted toward the red. This effect can be much more pronounced for short-lived emitters and much less pronounced for long-lived emitters.

### Spectral analysis

We prepared solutions of Rh and Ru in water. These two dyes easily mix and do not interact. Therefore, the observed emission is a simple sum of the two emissions.[3] In Figure 8(A), we present the normalized steady-state emission spectra of Rh and Ru in solution. In contrast, Figure 8(B) shows the emissions for different mixes containing a different relative amount of background (Rh) and probe (Ru) as measured with single-pulse excitation. The solid black line represents the measurement for an approximately 50:50 mixture of contributing signals. The solid blue line represents the measured signal where the background constitutes ~90% of the total signal, and the solid red line is the measured signal from the mix where the background constitutes about 98% of the total signal. From the measured, steady-state signals, it is already clear that the 10% signal contribution of the probe is difficult to be distinguished from the overall emission spectrum. Furthermore, the spectrum of only 2% of probe contribution is almost identical to the background.

In Figure 9, we present the emission spectra for the same solution as measured with one, three, and eight pulses bursts, respectively, where the collection of photons was initiated with the last pulse and the integration time was shorter than the arrival time of a subsequent pulse burst. Therefore, for Ru (fluorescence lifetime of 300 ns), we used a burst of pulses at a fundamental internal repetition rate of 40 MHz and an external repetition rate between bursts of 500 kHz. The photons are counted up to 700 ns, which is sufficient for Ru to almost completely decay. The spectra measured with a single pulse correspond well to the measured steady-state emission spectra. In fact, these are time-resolved emission spectra (TRES) for a zero-time delay. For the highest concentration

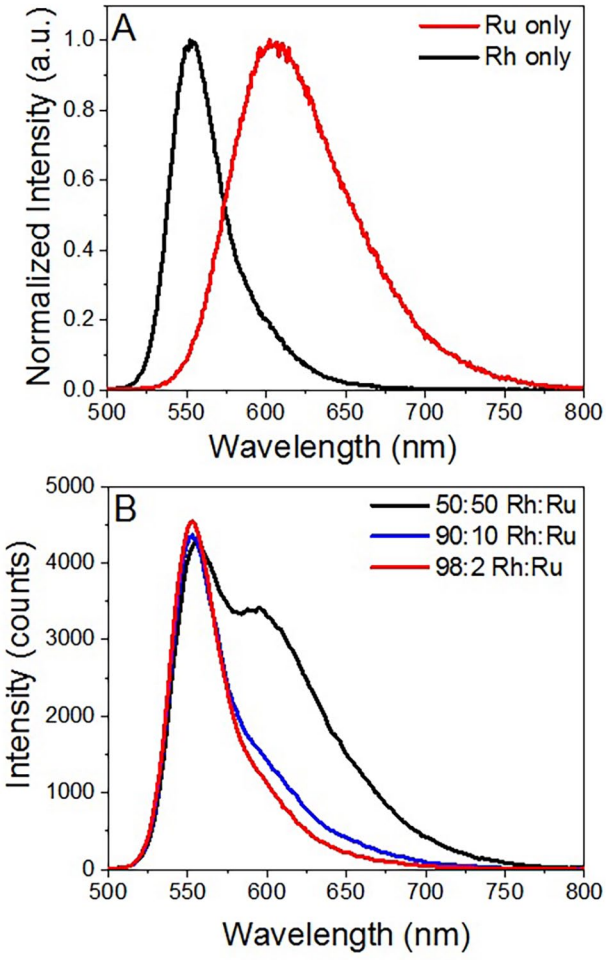


**Figure 8.** Normalized steady-state emission spectra of Rh and Ru in solution (A), and emissions for different mixes containing a different relative amount of background (Rh) and probe (Ru) as measured with single-pulse excitation (B). (A color version of this figure is available in the online journal.)

of the probe Ru, the spectra with three and eight pulses are clearly dominated by the probe emission. For the second concentration of the probe, we can clearly see the presence of probe emission, and for eight pulses, the total emission spectrum is very similar to the 50:50 sample measured with a single pulse. For the lowest contribution of the probe, the improvement is proportional, and for eight pulses, the overall emission spectrum corresponds to the 90:10 mix steady-state spectrum.

In Figure 10, we present the differential spectra for all six cases. It is clear that the obtained spectra resemble the probe emission very well. The differential emission spectra measured with eight pulses are about 50% higher than the spectra measured with three pulses bursts.

For comparison, in Figure 11, we present the normalized differential emission spectra (three pulses – one pulse and eight pulses – one pulse) overlaid with just the probe (Ru) steady-state emission. The agreement is very good, but a small, long wavelength shift of the emission can be observed. Even though this was initially a little confusing, we must realize that exciting with eight pulses generates a much larger population of relaxed molecules that are expected to contribute to longer emission wavelengths. The expected shift for a probe with a shorter fluorescence lifetime would be significantly greater.

These experiments confirm that a simple spectra subtraction precisely yields the emission of the long-lived probe even when the contribution of the probe is negligible as compared to the background signal. Since with three pulses, the overall signal of the probe increases about 2.7-fold, this signal is 2.7 times higher than the signal measured with a single pulse. And for eight pulses, it is almost five times higher.

### Image analysis

Next, we tested the limits of the presented technology in simple imaging using a model system. For imaging, it is convenient to spatially separate the short-lived and long-lived emitters. The analysis of a solution mix with highly overlapping emission spectra would not be sufficiently convincing. To generate spatially separated signals of background and probe, we embedded Rh and Ru into polyvinyl alcohol (PVA) films. In this way, we can have a simple strip of PVA film of Rh with a fluorescence lifetime $<5$ ns and a strip of film containing Ru with a long fluorescence lifetime of about 1 μs. To protect the PVA films from the water environment, we laminated them. Such films can be easily inserted in a water-based environment for an extended period of time without worrying about the film dissolving and the probe leaking into the solution.

First, we placed the two polymer films next to each other, as shown in the photographs reported in Figure 12(A) and (B). Figure 12(A) is a photograph of the entire setup, showing the laser illumination through fiber optics (excitation), the blue illuminated spot on the Petri dish, and the camera objective (detection). The signal from the film containing Rh is significantly stronger than the signal from the film containing Ru. Such a configuration of films can be imaged by a time-gated camera. For our experiment, we used a PI-MAX 4 (Princeton Instruments, Inc., Trenton, NJ, USA) camera with $1024 \times 1024$ pixels resolution. Both strips were illuminated with a laser excitation (375 nm) through the fiber optics, as shown in Figure 12(A). On the observation line of the camera, we used a long-pass filter of 550 nm to eliminate the scattered excitation light. Both emissions of Rh and Ru are transmitted easily through the filter. The camera is triggered with the last pulse in the burst. In practice, the triggering time of the camera can be delayed electronically or just using a different length of the connecting cable. The image captured with a single pulse is presented in Figure 12(C). Both strips are visible, including the bright edges of the lamination film. This is a typical artifact due to the propagation of the emission light toward the edge of the film that appears brighter than the bulk film. In Figure 12(D), we present the image as obtained with eight pulses. The scale of both images is automatically adjusted by the camera to the brightest pixel. After eight pulses, the signal from Ru becomes significantly brighter and the Ru strip becomes more visible in the second picture. In Figure 12(E), we present the differential image between eight pulses and one pulse. We see the Ru PVA strip while the Rh strip and the background disappear.

In Figure 13(A), we use a large piece of Rh film on which we positioned two Ru strips. The Rh film serves to simulate an undesired background signal. In Figures 13(B) and (C), we present the images obtained with one and eight pulses,

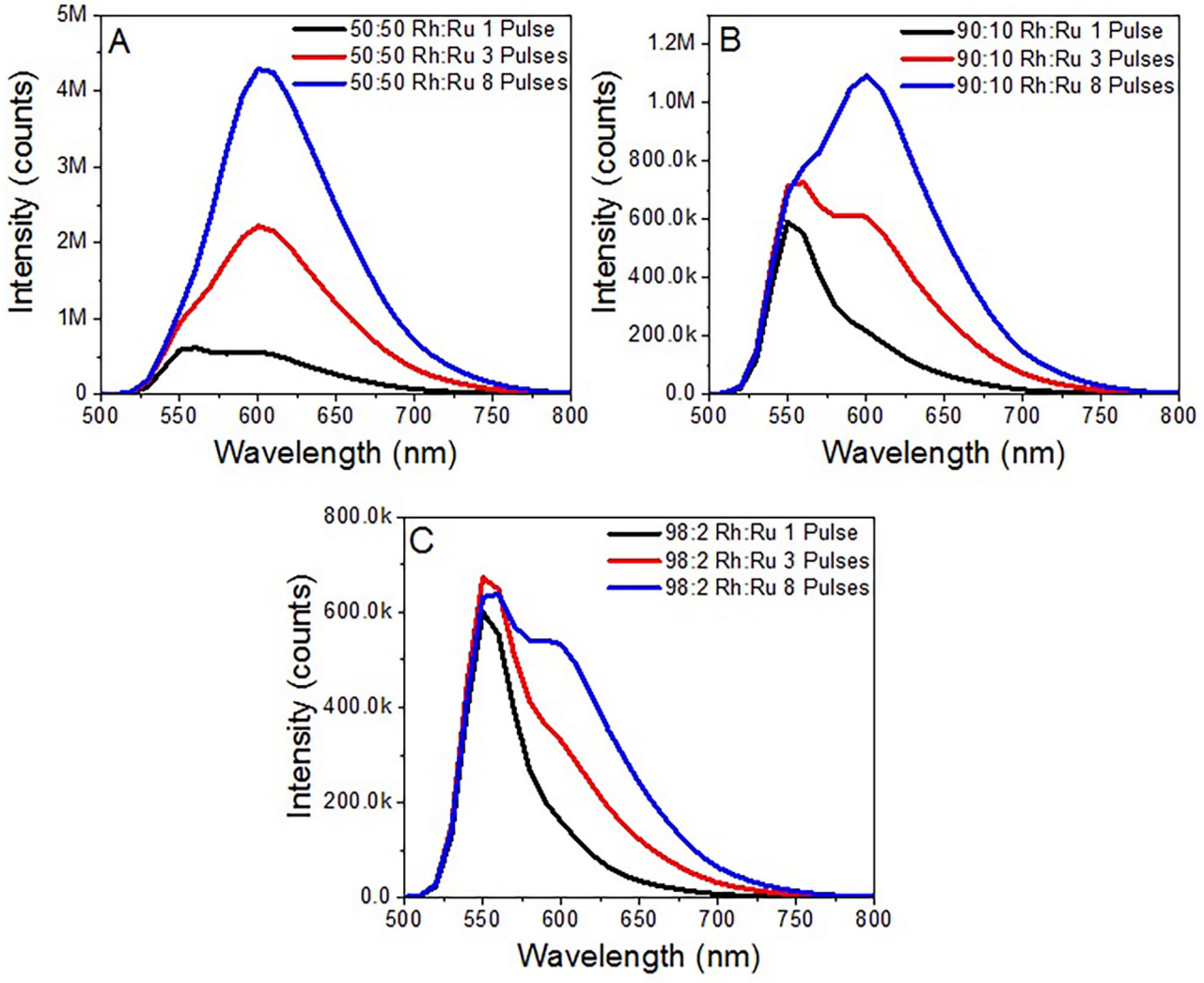


**Figure 9.** Emission spectra for a 50:50 (A), 90:10 (B), and 98:2 (C) signal contribution solution of Rh and Ru as measured with one, three, and eight pulses bursts. The collection of photons was initiated with the last pulse, and the integration time was shorter than the arrival time of a subsequent pulse burst. (A color version of this figure is available in the online journal.)

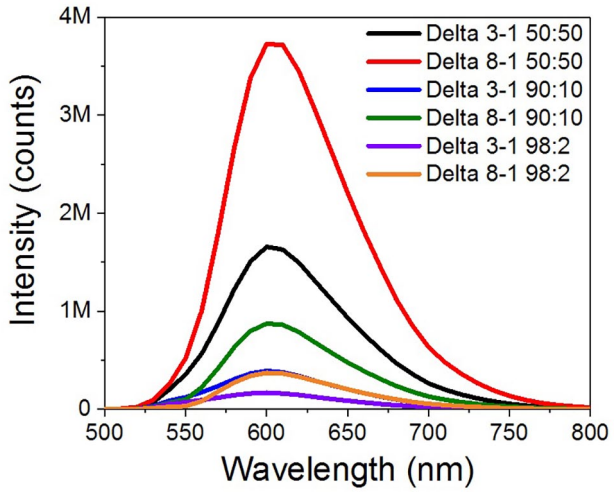


**Figure 10.** Differential spectra for the three Rh and Ru solutions (50:50, 90:10, and 98:2) obtained by subtracting the signal with one pulse from the signals with eight and three pulses. (A color version of this figure is available in the online journal.)

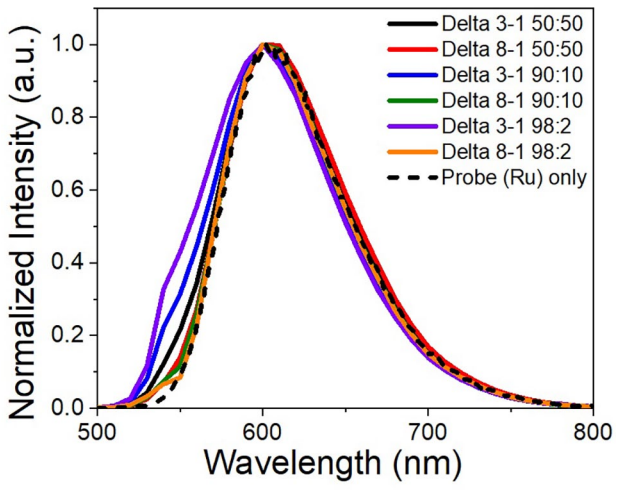


**Figure 11.** Normalized differential spectra for the three Rh and Ru solutions (50:50, 90:10, and 98:2) obtained by subtracting the signal with one pulse from the signals with eight and three pulses. (A color version of this figure is available in the online journal.)

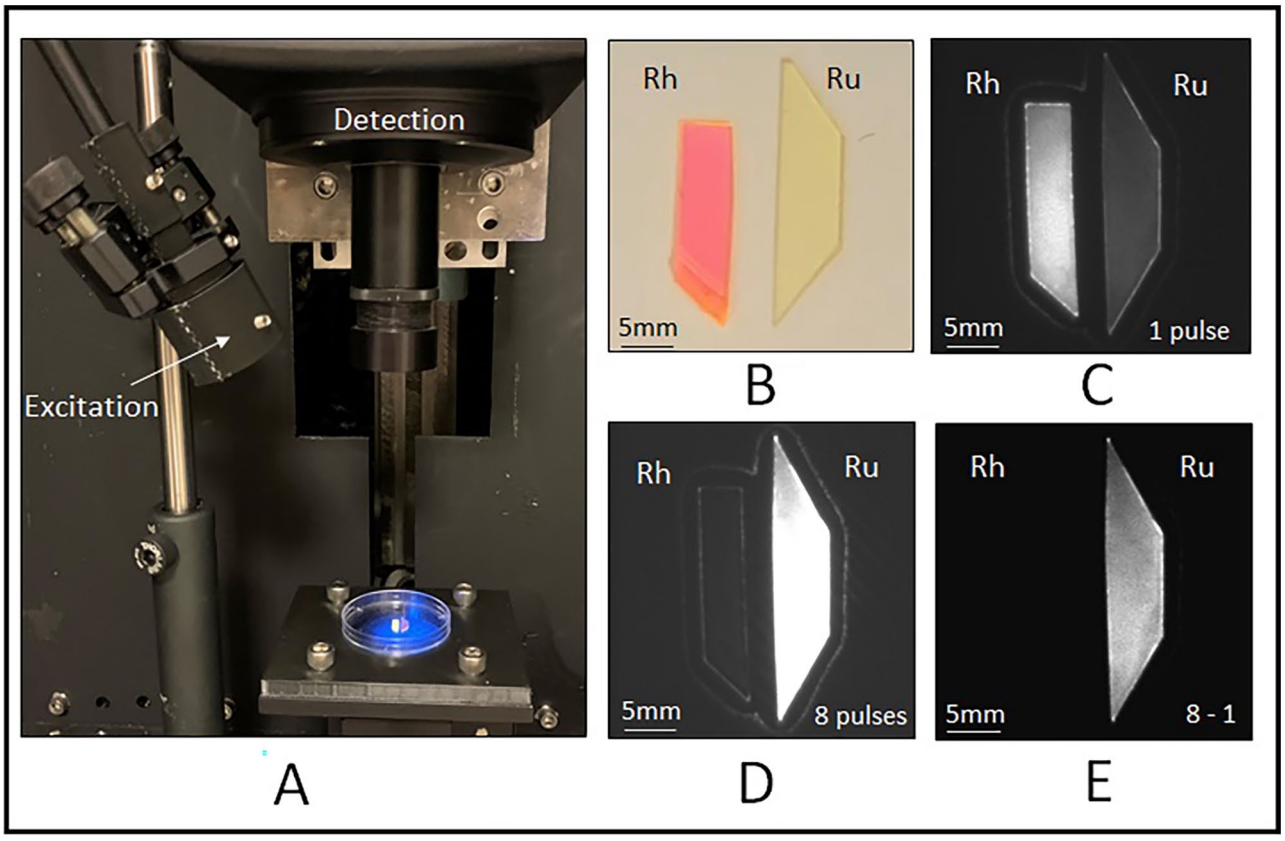


**Figure 12.** Imaging setup of the two films of Rh and Ru placed in a Petri dish (A), photograph of the films (B), image captured with a single pulse (C), image obtained with eight pulses (D), and differential image (E). The scale bar is 5 mm. (A color version of this figure is available in the online journal.)

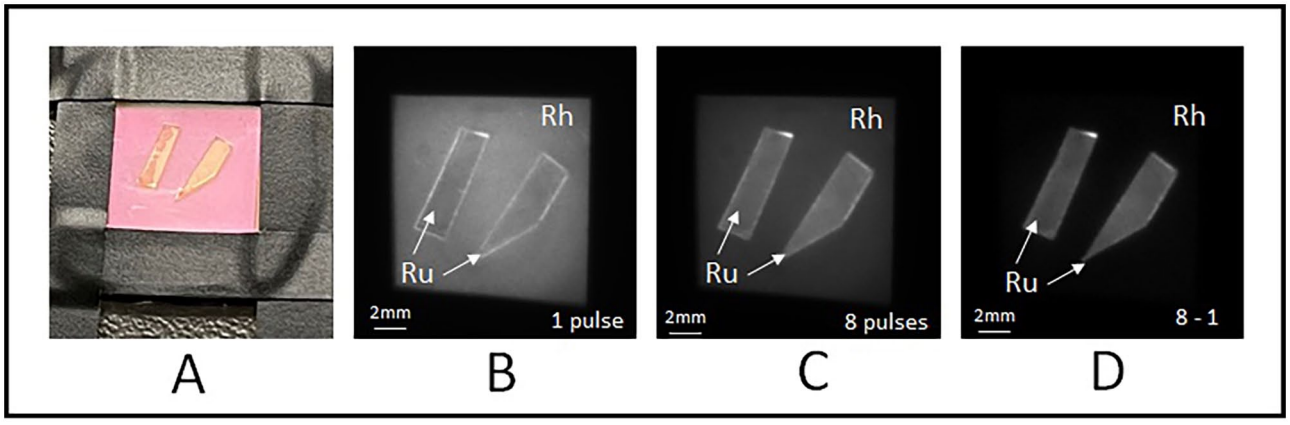


**Figure 13.** Imaging setup of a large piece of Rh film on which we positioned Ru strips. Photograph of the sample (A), image obtained with one pulse (B), image obtained with eight pulses (C), and differential image (D). The scale bar is 2 mm. (A color version of this figure is available in the online journal.)

respectively. The image captured with one pulse shows a bright signal from the Rh background. Differently, the image captured with eight pulses more evidently shows the signal coming from the Ru strips. The differential image is shown in Figure 13(D). The background is successfully removed, and a clear signal from the Ru strips is visible.

A common problem with cellular and tissue imaging is scattering, which greatly limits the penetration depth and image resolution. Scattering is a very fast process, and the presented technology should effectively eliminate scattering of the excitation light and scattering of background emission. A typical delay for scattered photons emitted by the Rh film that diffuse in the media will be negligible compared to the pulse separation in the burst.

To demonstrate the scattering effect, we used the PVA strips already shown in Figure 13. The PVA strips of Rh and Ru are submerged in different depths of intralipid (IL) solution (50× dilution). IL is commonly used to simulate a scattering environment in biological samples.[44–47] The utilized IL is a 20% emulsion of phospholipid-stabilized soybean oil. It was purchased by Sigma-Aldrich (St. Louis, MO, USA) and diluted 50 times for our experimental use. We want to stress

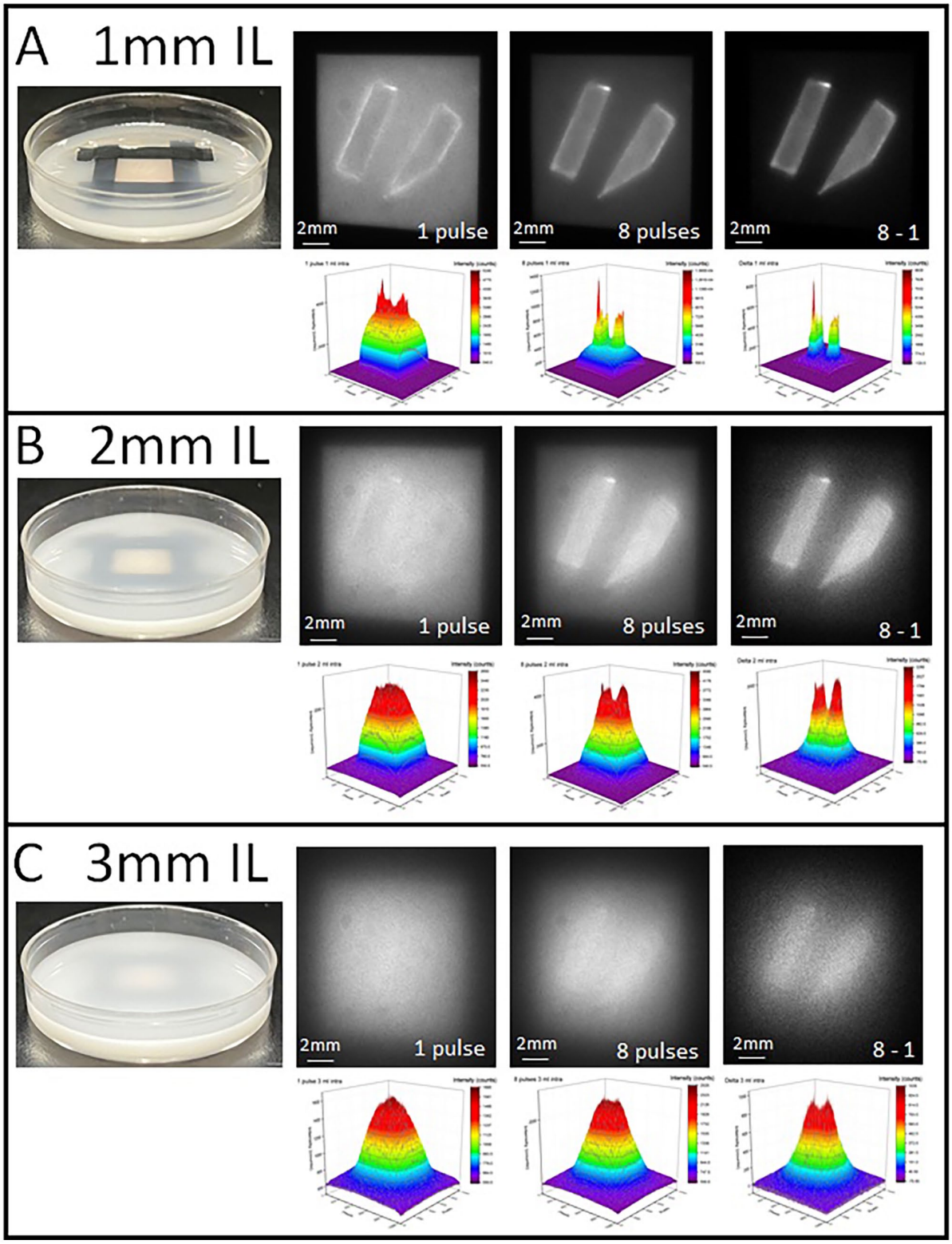


**Figure 14.** Images obtained from samples submerged in different amounts of intralipid solution, 1 mL (1 mm) (A), 2 mL (2 mm) (B), and 3 mL (3 mm) (C). The inset shows a real photograph of the sample for each amount of intralipid. A 3D intensity-based plot is also reported. The scale bar is 2 mm. (A color version of this figure is available in the online journal.)

that in our experiment, we used a short wavelength excitation of 375 nm that is much more prompt to scattering than NIR excitation. The penetration depth for blue excitation is significantly limited, and working with longer wavelength would greatly increase the excitation depth.

In Figures 14(A) to (C), we present samples submerged in different amounts of IL solution. For each amount of IL, we show a real photograph of the sample and three images, respectively, obtained with one pulse, eight pulses and by calculating the difference (8 pulses – 1 pulse). In Figure 14,

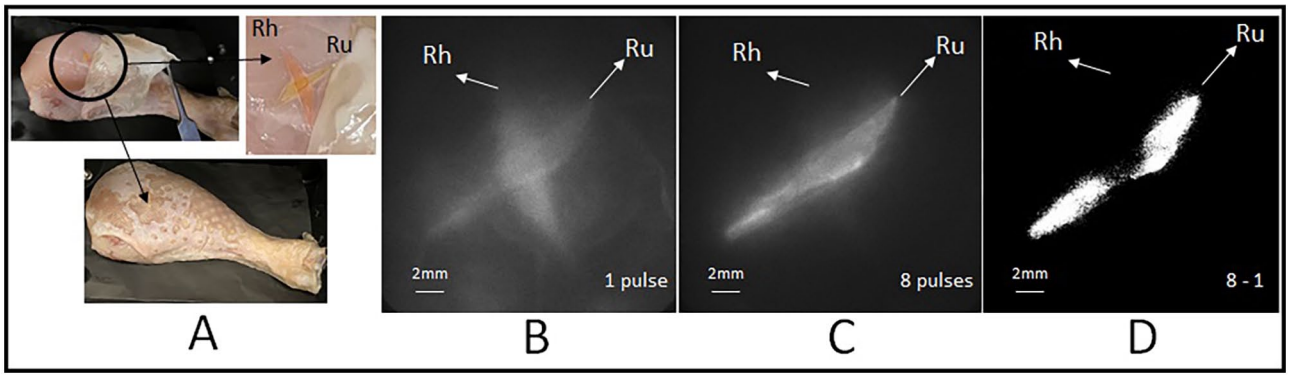


**Figure 15.** Sample containing the two strips of laminated Rh and Ru PVA films implanted under the skin of a chicken drumstick (A), image obtained with one pulse (B), image obtained with eight pulses (C), and differential image (D). The images were obtained using a 375-nm laser as excitation source. The scale bar is 2 mm. (A color version of this figure is available in the online journal.)

we also present a three-dimensional (3D) image intensity representation. As the IL depth increases, we can observe a blurring of the image, which significantly limits the resolution. This is expected since the photons emitted by the probe are scattered through the IL medium. For about 3 mm of IL solution over the sample, the strips separated by about 2 mm are difficult to be resolved. However, the pumped long-lived component (probe) is visible.

As a final demonstration, we used chicken skin. The sample containing the two strips of laminated PVA films was implanted under the skin of a chicken drumstick, as shown in the photograph in Figure 15(A).

The chicken drumstick was illuminated with a 375-nm laser. We want to stress that this excitation wavelength is suitable for the excitation of Ru but has a very limited penetration depth in the tissue and stimulates a great amount of intrinsic autofluorescence. A single-pulse image and an eight pulse burst image are presented in Figures 15(B) and (C), respectively. Despite the film being covered by a layer of about 3 mm of skin, the differential image (Figure 15(D)) clearly shows the Ru strip. This proves the effectiveness of the described method in detecting the signal from a sample deeply embedded into a highly scattering and intrinsic fluorescent tissue.

## Conclusions

Early detection of a disease is a key element to a successful treatment. Fluorescence imaging is an emerging diagnostic modality that has the potential for sensitive and minimally invasive detection and localization of various malignant diseases. Rapid advancements in fluorescent probes development, molecular designs, drug formulation, and drug delivery strategies continuously open additional possibilities for detection, diagnostic, and imaging. The future clinical role of fluorescence imaging will greatly depend on the development of new detection technologies and the design of detection instruments that can be easily adapted to practical situations.[45]

In this contribution, we described a novel approach that utilizes long fluorescence lifetimes and excitation pulse manipulation (multipulse sequences) to significantly increase the signal-to-background ratio (SBR) and immensely improve detection sensitivity. The presented approach can easily be implemented into practical tissue and microscopy imaging technologies. When combined with time-gated detection, this technique can easily achieve two orders increase in detection sensitivity.[7] This technology can be used with any long-lived luminophore, including potential uses of phosphorescence.

### AUTHORS' CONTRIBUTIONS

All authors participated in the design, interpretation of the studies and analysis of the data, and review of the manuscript. LC, JC, and JK conducted the experiments. ZG, LC, and EK wrote the manuscript. LC, ZG and IG designed the experimental part. The manuscript was reviewed and edited by all authors.

### ACKNOWLEDGEMENTS

The author (ZG) acknowledges the support from "Tex" Moncrief Jr. and TCU College of Science and Engineering.

### DECLARATION OF CONFLICTING INTERESTS

The author(s) declared no potential conflicts of interest with respect to the research, authorship, and/or publication of this article.

### FUNDING

The author(s) received no financial support for the research, authorship, and/or publication of this article.

### ORCID IDS

Luca Ceresa https://orcid.org/0000-0001-8771-496X
Joseph Kimball https://orcid.org/0000-0001-5869-4883

### REFERENCES

1. Jameson DM. *Introduction to fluorescence*. Abington: Taylor & Francis/CRC Press, 2014
2. Lakowicz JR. *Principles of fluorescence spectroscopy*. 3rd ed. Berlin: Springer, 2006
3. Gryczynski Z, Gryczynski I. *Practical fluorescence spectroscopy*. Abington: Taylor & Francis/CRC Press, 2020
4. Valeur B, Berberan-Santos MN. *Molecular fluorescence: principles and applications*. Weiheim: Wiley-vch Verlag Gmbh & Co. Kgaa, 2012
5. Maliwal BP, Fudala R, Raut S, Kokate R, Sørensen TJ, Laursen BW, Gryczynski Z, Gryczynski I. Long-lived bright red emitting azaoxotriangulenium fluorophores. *PLoS ONE* 2013;**8**:e63043

6. Sorensen TJ, Thyrhaug E, Szabelski M, Gryczynski I, Gryczynski Z, Laursen BW. AzadioxaTriAnulenium: a long fluorescence lifetime fluorophore for large biomolecule binding assay. *Methods Appl Fluoresc* 2013;**1**:25001
7. Kimball JD, Maliwal B, Raut S, Doan H, Nurekeyev Z, Gryczynski I, Gryczynski Z. Enhanced DNA detection using a multiple pulse pumping scheme with time-gating (MPPTG). *Analyst* 2018;**143**:2819–27
8. Hazlett TL, Johnson AE, Jameson DM. Time-resolved fluorescence studies on the ternary complex formed between bacterial elongation factor Tu, guanosine 5′-triphosphate, and phenylalanyl-tRNAph. *Biochemistry* 1989;**28**:4109–17
9. Kalayanasundarm K. *Photochemistry of polypyridine and porphyrin complexes*. New York: Academic Press, 1992.
10. Juris A, Balzani V, Barigelletti F, Campagna S, Belser P, Von Zelewsky A. Ru(II) polypyridine complexes: photophysics, photochemistry, eletrochemistry, and chemiluminescence. *Coord Chem Rev* 1988;**84**:85–277
11. Tyson DS, Castellano FN. Intramolecular singlet and triplet energy transfer in a Ruthenium(II) Diimine complex containing multiple Pyrenyl chromophores. *J Phys Chem A* 1999;**103**:10955–60
12. Maliwal B, Gryczynski Z, Lakowicz J. Long-wavelength long-lifetime luminophores. *Anal Chem* 2001;**73**:4277–85
13. Raut SL, Fudala R, Rich R, Kokate RA, Chib R, Gryczynski Z, Gryczynski I. Long lived BSA Au clusters as a time gated intensity imaging probe. *Nanoscale* 2014;**6**:2594–7
14. Shang L, Dong S, Nienhaus GU. Ultra-small fluorescent metal nanoclusters: synthesis and biological applications. *Nano Today* 2011;**6**:401–18
15. Charbonnière LJ, Hildebrandt N, Ziessel RF, Löhmannsröben HG. Lanthanides to quantum dots resonance energy transfer in time-resolved fluoro-immunoassays and luminescence microscopy. *J Am Chem Soc* 2006;**128**:3912800–9
16. Leif R, Clay SP, Gratzner HG, Haines HG, Rao KV, Vallarino LM. The automation of uterine cancer cytology. In: Wied GL, Bahr GF, Bartels PH (eds) Tutorials of cytology. Chicago, IL: Tutorials of Cytology, 1976, pp.313–44
17. Jin D, Piper JA. Time-gated luminescence microscopy allowing direct visual inspection of lanthanide-stained microorganisms in background-free condition. *Anal. Chem* 2011;**83**:2294–300
18. Liu Y, Tu D, Zhu H, Ma E, Chen X. Lanthanide-doped luminescent nano-bioprobes: from fundamentals to biodetection. *Nanoscale* 2013;**5**:1369–84
19. May A, Bhaumik S, Gambhir SS, Zhan C, Yazdanfar S. Whole-body, real-time preclinical imaging of quantum dot fluorescence with time-gated detection. *J Biomed Opt* 2009;**14**:060504
20. Saviotti M, Galley W. Room temperature phosphorescence and the dynamic aspects of protein structure. *Proc Natl Acad Sci USA* 1974;**71**:4154–8
21. Geacintov NE, Brenner HC. The triplet state as a probe of dynamics and structure in biological macromolecules. *Photochem Photobiol* 1989;**50**:841–58
22. Schlyer B, Schauerte J, Steel D, Gafni A. Time-resolved room temperature protein phosphorescence: nonexponential decay from single emitting tryptophans. *Biophys J* 1994;**67**:1192–202
23. Kenry CC, Liu B. Enhancing the performance of pure organic room temperature phosphorescent luminophores. *Nature Com* 2019;**10**:2111
24. Strickler SJ, Berg RA. Relationship between absorption intensity and fluorescence lifetime of molecules. *J Chem Phys* 1962;**37**:814–22
25. Frangioni JV, The problem is background not signal. *Mol Imag* 2009;**8**:00033
26. Soubret A, Ntziachristos V. Fluorescence molecular tomography in the presence of background fluorescence. *Phys Med Biol* 2006;**51**:3983–4001
27. Richards-Kortum R, Sevick-Muraca E. Quantitative optical spectroscopy for tissue diagnosis. *Annu Rev Phys Chem* 1996;**47**:555–606
28. Daehne S, Resch-Genger U, Wolfbeis OS. *Near-infrared dyes for high technology applications* (ed S Daehen). Amsterdam: Kluwer Academic Publishers, 1998.
29. Vahrmeijer AL, Hutteman M, van der Vorst JR, van de Velde CJH, Frangioni JV. Image-guided cancer surgery using near-infrared fluorescence. *Nat Rev Clin Oncol* 2013;**10**:507–18
30. Sevick-Muraca E. Translation of near-infrared fluorescence imaging technologies. *Annu Rev Med* 2012;**63**:217–31
31. Gross S, Piwnica-Worms D. Real-time imaging of ligand induced IKK activation in intact cells and in living mice. *Nat Methods* 2005;**2**:607–14
32. Contag CH, Jenkins D, Contag PR, Negrin RS. Use of reporter genes for optical measurements of neoplastic disease in vivo. *Neoplasia* 2000;**2**:41–52
33. Zong C, Wu J, Liu M, Yang L, Yan F, Ju H. Chemiluminescence imaging for a protein assay via proximity-dependent DNAzyme formation. *Anal Chem* 2014;**8619**:9939–44
34. Bhaumik S, Gambhir SS. Optical imaging of Renilla luciferase reporter gene expression in living mice. *Proc Natl Acad Sci USA* 2002;**99**:377–82
35. Levitt JA, Matthews DR, Ameer-Beg SM, Suhling K. Fluorescence lifetime and polarization-resolved imaging in cell biology. *Curr Opin Biotechnol* 2009;**20**:28–36
36. Elson D, Requejo-Isidro J, Munro I, Siegel FRJ, Suhling K, Benninger PTR, Lanigan P, McGinty J, Talbot C, Treanor B, Webb S, Sandison A, Wallace A, Davis D, Lever J, Neil M, Phillips D, Stamp G, French P. Time-domain fluorescence imaging applied to biological tissue. *Photochem Photobiol Sci* 2004;**3**:795–801
37. Rich RM, Stankowska DL, Maliwal BP, Sorensen TJ, Laursen BW, Krishnamoorthy RR, Gryczynski Z, Borejdo J, Gryczynski I, Fudala R. Elimination of autofluorescence background from fluorescence tissue images by use of time-gated detection and the AzaDiOxaTriAngulenium (ADOTA) fluorophore. *Anal Bioanal Chem* 2013;**405**:2065–75
38. Chib R, Requena S, Mummert M, Strzhemechny YM, Gryczynski I, Borejdo J, Gryczynski Z, Fudala R. Fluorescence lifetime imaging with time-gated detection of hyaluronidase using a long lifetime azadioxatriangulenium (ADOTA) fluorophore. *Methods Appl Fluoresc* 2016;**174**:047001
39. Rich RM, Gryczynski I, Fudala R, Borejdo J, Stankowska DL, Krishnamoorthy RR, Raut S, Maliwal BP, Shumilov D, Doan H, Gryczynski Z. Multiple-pulse pumping for enhanced fluorescence detection and molecular imaging in tissue. *Methods* 2014;**66**:292–8
40. Shumilov D, Rich RM, Gryczynski I, Raut S, Gryczynski K, Kimball J, Doan H, Sørensen TJ, Laursen BW, Borejdo J, Gryczynski Z. Generating multiple-pulse bursts for enhanced fluorescence detection. *Methods Appl Fluoresc* 2014;**2**:024009
41. Multi-pulse pumping for enhanced fluorescence detection and molecular imaging in cells and tissue. US Patent # US9612245 B**2**, 2017.
42. Muller BK, Zaychikov E, Brauchle C, Lamb DC. Pulsed interleaved excitation. *Biophys J* 2005;**86**:3508–22
43. Ruettinger S, Buschmann V, Kraemer B, Orthaus S, Koberling F. FRET analysis with Pulses Interleaved Excitation (PIE) using the Microtime 200, https://www.picoquant.com/images/uploads/page/files/7266/appnote_pie-fret.pdf
44. Grecco HE, Lidke KA, Heintzmann R, Lidke DS, Spagnuolo C, Martinez OE, Jares-Erijman EA, Jovin TM. Ensemble and single particle photophysical properties (two-photon excitation, anisotropy, FRET, lifetime, spectral conversion) of commercial quantum dots in solution and in live cells. *Microsc Res Tech* 2004;**65**:169–79
45. Anderson-Engels S, Svenberg K, Svenberg S. Fluorescence imaging in medical diagnostics. In: Fujimoto JG and Farkas DL (eds) *Biomedical optical imaging*. Oxford: Oxford University Press, 2009, pp.265–305
46. Abugo OO, Gryczynski Z, Lakowicz JR. Modulation sensing of fluorophores in tissue: a new approach to drug compliance monitoring. *J Biomed Opt* 1999;**4**:429–42
47. Gryczynski Z, Abugo OO, Lakowicz JR. Polarization sensing of fluorophores in tissues for drug compliance monitoring. *Anal Biochem* 1999;**273**:204–11